Numerical Analysis of Attached Turbulent Boundary Layers Along Strongly Curved Surfaces

A. Eghlima* and C. Kleinstreuer†
Rensselaer Polytechnic Institute, Troy, New York

The problem of steady incompressible turbulent flow past two-dimensional or axisymmetric bodies with strong longitudinal and transverse curvature effects is solved numerically for the region where the streamlines stay approximately parallel to the wall. Although predictive computer simulation models for such flow systems exist, published simulation results fall short in matching measured local and integral properties of thick turbulent boundary layers. The main reason for the observed discrepancies lies in the use of inappropriate modeling equations. The computer simulation results based on a new set of higher-order boundary-layer equations with zero-equation turbulence model are in excellent agreement with experimental observations for two different afterbodies.

Nomenclature

A = Van Driest damping factor
a = turbulence structure coefficient
b,c = correlation factors
f = dimensionless streamfunction
h = metric coefficient, $=1+Kn$
K = longitudinal curvature, $1/R$
L = turbulence length scale
L_r = reference length
ℓ_m = mixing length
M = geometric factor, $r^i - r_o{}^i(1-h^j)$
n = coordinate normal to body
p = pressure
$\bar{p}$ = nondimensional pressure
$Q_1,\ldots,Q_{15}$ = parameters in Eq. (29)
R = radius of longitudinal curvature
r = transverse radius of curvature, $=r_o+n\cos\theta$
r_o = transverse radius of curvature of the body
$r_{\max}$ = maximal radius of test body
s = coordinate along the body surface
$\bar{s}$ = nondimensional coordinate along the body surface
t = time
u,v = s and n component of the velocity, respectively
$\bar{u},\bar{v}$ = dimensionless velocity in s and n directions, respectively
$\bar{u},\bar{v}$ = time-averaged velocity in s and n directions, respectively
u',v' = velocity fluctuation in s and n directions, respectively
$\rho\bar{u'^2},\rho\bar{v'^2}$ = Reynolds normal stress in s and n directions, respectively
u_∞ = outer potential flow velocity
U_∞ = approach velocity
u_e = velocity at boundary-layer edge
U = dimensionless variable, $=\partial f/\partial\eta$
V = nondimensionless variable, $\equiv\partial U/\partial\eta$
$\rho\overline{u'v'}$ = Reynolds shear stress
α = correlation factor
β_c = longitudinal curvature effect parameter
γ_{tr} = intermittency factor
θ = angle between axis of symmetry and tangent to the surface
τ = shear stress
ν = kinematic viscosity
ν_t = eddy viscosity
μ = dynamic viscosity
ρ = mass density
ζ = vorticity vector
ξ = transformed s coordinate
η = nondimensional transformed n coordinate
δ = boundary-layer thickness
ϵ_m = nondimensonal eddy viscosity, $=\nu_t/\nu$

Superscripts

i = transverse curvature index, = 1 does exist, = 0 does not exist
j = longitudinal curvature index, = 1 does exist, = 0 does not exist

Subscripts

e = outer edge of boundary layer
f = flat plate
i = inner
o = outer
t = turbulent
tr = transition

Received Nov. 16, 1983; revision received April 24, 1984.

*Research Associate.
†Associate Professor, Department of Mechanical & Aerospace Engineering, North Carolina State University, Raleigh, N.C.

Introduction

CHARACTERISTICS of (turbulent) boundary layers in realistic external or internal flowfields are largely determined by longitudinal and transverse curvature effects, pressure gradients and additional rates of strain, as well as by flow separation and wake formation. Examples include flow around ship hulls or airfoils and flow in bent diffusors. For such systems, the laminar/turbulent boundary layer may become thick and, in addition, strong interactions between the inner viscous flow and the outer potential flow develop.

Accurate prediction of the viscous drag along a body of revolution and the associated velocity profiles requires solving mainly (the) higher-order boundary-layer equations for submerged bodies in a flowfield with nonuniformities. At the high Reynolds numbers of interest, the analysis involves the usual difficulties encountered with turbulent boundary layers in a pressure gradient now accentuated by the boundary-layer thickness (relative to the transverse and/or longitudinal body radius). Van Dyke[1,2] has shown that longitudinal curvature

makes a contribution that is additive to that of transverse curvature and of the same relative order. Meroney and Bradshaw[3] have measured turbulent boundary-layer growth in a prolonged bend, and based on their conclusions for a convex surface, a small change in curvature ($\delta/R \approx 0.01$) arouses a large 10% change in the integral properties of the flowfield (e.g., the skin friction coefficient). Different investigators[4-9] have used different methods to solve thick boundary-layer problems for special situations by taking into account some of the nonuniformities, such as longitudinal or transverse curvature effects, normal stresses, pressure variations across the boundary layer, or the effect of thickening on turbulence models, but not all of them as done in this paper. On the other hand, Kleinstreuer et al.[10] showed that the momentum equation usually employed for calculating longitudinal curvature effects[2] cannot fully represent the influence of strongly curved surfaces on the growth of thick boundary layers. Curvature effects on laminar and turbulent boundary-layer flow parameters were measured by several researchers.[3,11-17]

We are presenting higher-order boundary-layer equations that simulate steady, incompressible, axisymmetric, turbulent flowfields more accurately than with existing models which rely on incomplete sets of equations and, in some cases, strongly on semiempirical submodels to compensate for difficiencies in the governing equations. For example, Cebeci et al.[6] employed the turbulent version of Van Dyke's higher-order boundary-layer equations plus one extra third-order term but could not predict experimental data[16] accurately for longitudinal curvature flow along a bend. Wang and Huang[18] employed the C-S Douglas code[19] enhanced by a correction factor[7] to the eddy viscosity based on measurements. The pressure variation is usually obtained by potential flow calculations for the final displacement body or is based on measurements, i.e., most investigators[5-8] ignore the momentum equation in normal direction for computing the pressure gradient.

Analysis

System Conceptualization and Modeling Equations

The schematics of steady incompressible flow near the tail of a planar or axisymmetric body are shown in Fig. 1. Region I is characterized by the fact that the mean flow streamlines remain nearly parallel to the rigid surface, i.e, $v \ll u$. In region II it is no longer possible to assume that $v \ll u$ since the streamlines do not stay parallel to the body surface. Due to the thickening of the boundary layer, (strong) interactions between the viscous flow domain and region III can be expected. Depending upon the magnitude of the Reynolds number and the geometry of the submerged body, the condition of region II, i.e., $v = \mathcal{O}(u)$, might already be important before separation.

In restricting the analysis to steady, incompressible two-dimensional or axisymmetric flow without separation past a submerged body or within conduits, we can make particular use of the orthogonal coordinate system (s,n) as shown in Fig. 1. Here, n is the distance normal to the (curved) body surface and s the distance measured along the surface starting with the stagnation point, for example. With these assumptions, the general conservation equations for fluid mass and momentum may be written for the curvilinear coordinate system as

$$\frac{\partial}{\partial s}(ur) + \frac{\partial}{\partial n}(vrh) = 0 \tag{1}$$

$$\frac{u}{h}\frac{\partial u}{\partial s} + v\frac{\partial u}{\partial n} + \frac{uvK}{h} = -\frac{1}{\rho h}\frac{\partial p}{\partial s} + \nu\left\{\frac{1}{h^2}\frac{\partial^2 u}{\partial s^2} + \frac{\partial^2 u}{\partial n^2} + \frac{1}{rh} \times \left[\frac{\partial}{\partial s}\left(\frac{r}{h}\right)\frac{\partial u}{\partial s} + \frac{\partial}{\partial n}(hr)\frac{\partial u}{\partial n}\right]\right\} \tag{2}$$

$$\frac{u}{h}\frac{\partial v}{\partial s} + v\frac{\partial v}{\partial n} - \frac{Ku^2}{h} = -\frac{1}{\rho}\frac{\partial p}{\partial n} + \nu\left\{\frac{1}{h^2}\frac{\partial^2 v}{\partial s^2} + \frac{\partial^2 v}{\partial n^2} + \frac{1}{rh} \times \left[\frac{\partial}{\partial s}\left(\frac{r}{h}\right)\frac{\partial v}{\partial s} + \frac{\partial}{\partial n}(hr)\frac{\partial v}{\partial n}\right]\right\} \tag{3}$$

where the geometric parameters $h = 1 + 1/R$ and $K = 1/R$ reflect longitudinal curvature effects whereas $r = r_o + n\cos\theta$ accommodates the transverse curvature. The system of Eqs. (1-3) can be simplified for distinct parts of the flow domain employing the relative order of magnitude analysis as outlined in Ref. 10.

New Parabolic Modeling Equations and Turbulence Models for Flow Region I

Region I is defined as a subdomain where the mean flow streamlines remain nearly parallel to the surface regardless of the relative thickness of the boundary layer. Hence, the normal component of the velocity vector v is significantly smaller than the longitudinal component u. With this assumption, we introduce dimensionless variables that are of the order of unity in the boundary layer as[2]

$$\tilde{u} = u/U_\infty \qquad \tilde{v} = Re^m v/U_\infty \qquad \tilde{s} = s/L_r$$
$$\tilde{n} = Re^m n/L_r \qquad Re = U_\infty L_r/\nu \qquad \tilde{p} = p/\rho U_\infty^2 \tag{4}$$

By substituting Eq. (4) into the system of Eqs. (1-3), expanding each term of the basic equations in negative powers of the Reynolds number and retaining only first- and second-order terms, we derived approximate equations where the physical representation of all terms is preserved individually. A detailed discussion and comparison with Van Dyke's[2] higher-order boundary equations is given by Kleinstreuer et al.[10]

After restoring the dimensional variables the new set of second-order boundary-layer equations reads

$$\frac{\partial}{\partial s}(r^i u) + \frac{\partial}{\partial n}[v(r^i - r_o^i(1-h^j))] + \mathcal{O}(Re^{-2m}) = 0 \tag{5}$$

$$(2-h^j)u\frac{\partial u}{\partial s} + v\frac{\partial u}{\partial n} + Kuv = -\frac{1}{\rho}(2-h^j)\frac{\partial \rho}{\partial s} + \nu\frac{\partial^2 u}{\partial n^2} + \nu\frac{\partial u}{\partial n}\frac{\partial}{\partial n}\left[\left(\frac{r}{r_o}\right)^i + h^j\right] + \mathcal{O}(Re^{-2m}) \tag{6}$$

$$Ku^2 = \frac{1}{\rho}\frac{\partial \rho}{\partial n} + \mathcal{O}(Re^{-2m}) \tag{7}$$

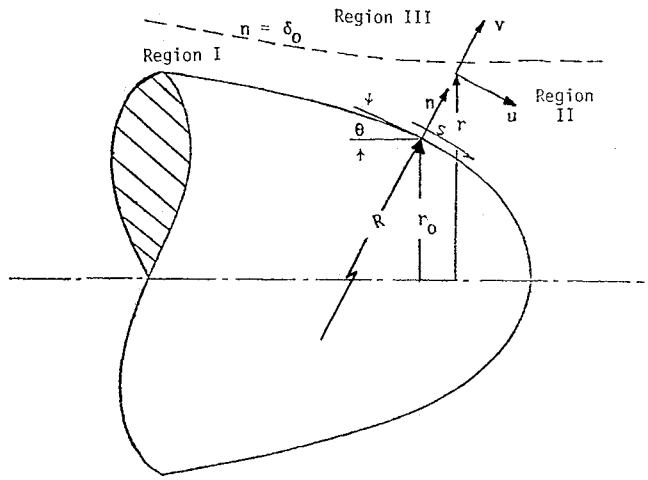

Fig. 1 Coordinate system and geometric parameters.

The flow indices i and j indicate the cases $i=j=0$ for flow past a flat plate; $i=1$, $j=0$ for axisymmetric bodies with no longitudinal curvature; and $i=0$, $j=1$ for flow without transverse curvature. Finally, $i=j=1$ when longitudinal and transverse curvature effects exist. The exponent $m=1/2$ for laminar and $m=4/5$ for turbulent thin boundary-layer flow with zero pressure gradient along a flat plate.

Splitting the instantaneous variables into time-smoothed and random components the turbulent flow version of the system of Eqs. (5-7) for region I reads[10]

$$\frac{\partial}{\partial s}(r^i\bar{u})+\frac{\partial}{\partial n}(\bar{v}M)=0 \tag{8}$$

$$(2-h^j)u\frac{\partial\bar{u}}{\partial s}+v\frac{\partial\bar{u}}{\partial n}+K\bar{u}\bar{v}=-\frac{1}{\rho}(2-h^j)\frac{\partial\bar{p}}{\partial s}+\frac{\partial^2\bar{u}}{\partial n^2}$$
$$+\frac{\partial\bar{u}}{\partial n}\frac{\partial}{\partial n}\left[\left(\frac{r}{r_o}\right)^i+h^j\right]-\frac{1}{M}\left[\left(\frac{M(2-h^j)+r}{2}\right)\frac{\partial}{\partial s}(\overline{u'^2})\right.$$
$$\left.+h^j\sin\theta(\overline{u'^2})+\frac{\partial}{\partial n^2}(\overline{u'v'}M)+KM(\overline{u'v'})\right] \tag{9}$$

$$K\bar{u}^2=\frac{1}{\rho}\frac{\partial\bar{p}}{\partial n}-K(\overline{u'^2}) \tag{10}$$

where $M=r^i-r_o^i(1-h^j)$, $K(1/R)^{1/j}$ and $\partial/\partial s(\overline{u'^2})\approx 0$ since $\overline{u'^2}$ is approximately constant in the streamwise direction for attached boundary layers.[20] This simplification which actually holds for flat-plate flow, makes Eq. (9) parabolic. An alternative approach for obtaining the turbulent flow modeling equations would be to apply the relative order of magnitude analysis to the exact Reynolds equations as given by Patel[21] and applied to flows past cylinders and cones. When this is done, an additional turbulence term, $\partial/\partial n\,(\overline{v'^2})$, appears in Eq. (10). When Eq. (10) is inserted into Eq. (9), $\partial/\partial n\,(\overline{v'^2})$ can be combined with $\partial/\partial n\,(\overline{u'v'})$ following Bradshaw's hypothesis that $\overline{u'v'}=a(\overline{u'^2}+\overline{v'^2}+\overline{w'^2})$; $\overline{v'^2}=b\overline{u'^2}$; and $\overline{w'^2}=c\overline{u'^2}$ where $0.13<a<0.2$, $0.4<b<0.8$, and $0.3<c<0.7$. It is interesting to note that a sensitivity analysis with our new equations indicated that any value within the given range of the turbulence structure coefficients does not affect the principle flow parameters noticeably. As shown below [Eq. (18)], absorbing $\partial/\partial n(\overline{v'^2})$ changes the coefficient α slightly which, in turn, also has negligible numerical effect on the system parameters.[22]

The associated boundary conditions are

$$\zeta=\nabla\times v=\frac{1}{h}\left[\frac{\partial v}{\partial s}-\frac{\partial(hu)}{\partial n}\right]=0 \tag{11}$$

which reflects the fact that the vorticity vanishes along the (unknown) edge of the boundary layer, i.e., the outer flow is irrotational. Substituting Eq. (4) into Eq. (11), restoring the original variables and neglecting terms of $\mathcal{O}(Re^{-2m})$ and higher, one obtains

$$\frac{\partial\bar{u}}{\partial n}+K\bar{u}=0 \tag{12a}$$

which integrated yields

$$\bar{u}=u_\infty(s)\exp[-nK(s)] \tag{12b}$$

where $u_\infty(s)$ is the outer potential flow velocity. In summary, for

$$n=0\rightarrow\bar{u}=0 \quad \text{and} \quad \bar{v}=0 \tag{13}$$

and for

$$n\geq\delta\rightarrow\bar{u}=u_\infty(s)\exp[-nK(s)] \tag{14}$$

The pressure variation along the edge of the displacement body is obtained with potential flow calculations using an iterative procedure discussed by Wang and Huang.[18] This displacement body concept is a relatively simple yet highly accurate method for calculating viscous-inviscid flow interactions for thick boundary layers with streamlines approximately parallel to the body surface. The n-momentum equation is then used to calculate the pressure gradient outward to the boundary-layer edge, assuming a constant (local) pressure within the thin displacement layer.

Equations (8-10) contain five unknowns, namely, $\bar{u}$, $\bar{v}$, $\bar{p}$, $\overline{u'v'}$, and $\overline{u'^2}$. In order to gain closure, it is, therefore, necessary to furnish some additional relationships. Based on the objective of computational efficiency and with the measured data sets found in the open literature, we incorporated an algebraic turbulence or zero-equation model for the shear stresses reflecting curvature effects and then related these expressions directly to the normal stresses. Among the algebraic submodels, the mixing length hypothesis (MLH) has proven very useful and realistic for a wide range of attached boundary-layer flows, provided that good choices are made for the mixing length distributions. Two commonly employed transport equations for turbulent shear stresses are the mixing length formula[23]

$$-\overline{u'v'}=\ell_m^2\left|\frac{\partial u}{\partial y}\right|\frac{\partial u}{\partial y} \tag{15}$$

and the eddy viscosity formula[24]

$$-\overline{u'v'}=\nu_t\frac{\partial u}{\partial y} \tag{16}$$

where $\nu_t=\nu_t(\ell_m)$ again. Following the method used for thin turbulent boundary-layer calculations, a composite layer consisting of two regions is postulated. The distributions of ℓ_m and ν_t are then described by two separate empirical expressions.

In general, the shear stresses are a function of mean-time velocity and velocity gradient as well as mixing lengths which, in turn, are dependent upon the radii of curvature, viz

$$\overline{u'v'}=\overline{u'v'}[\ell_m(R,r_o);\bar{u},\nabla\bar{u}] \tag{17}$$

The normal stresses are directly related to the shear stresses following Bradshaw's hypothesis

$$\overline{u'^2}=-\alpha\overline{u'v'};\ 2.2<\alpha<4.4 \tag{18}$$

In the inner boundary-layer region the eddy viscosity formula for submodel Eq. (16) can be expressed as[19]

$$(\nu_t)_i=\ell_{m,i}^2S^2\left(\frac{r}{r_o}\right)^i\left|\frac{\partial u}{\partial y}\right|\gamma_{\text{tr}} \qquad 0\leq y\leq y_c \tag{19}$$

where γ_{tr} is an intermittency factor; S incorporates the streamline curvature as postulated, for example, by Eide and Johnston[25]

$$S=1-\beta_c\left(\frac{u}{R}\right)\left(\frac{\partial u}{\partial y}\right)^{-1} \quad \text{with} \quad \beta_c=6\pm 4 \tag{20}$$

and $\ell_{m,i}$ is the inner mixing length for axisymmetric flow[19]

$$\ell_{m,i}=kr_o\ell n\left(\frac{r}{r_o}\right)\left\{1-\exp\left[-\frac{r_o}{A}\ell n\left(\frac{r}{r_o}\right)\right]\right\} \tag{21}$$

where $\beta_c\simeq 5.0$ is most appropriate,[22] $k=0.4$, and A is the damping length defined by Van Driest.[26]

For the outer boundary-layer region we adopted for the mixing length distribution of submodel Eq. (16) an expression postulated by Pletcher[27]

$$\ell_{m,o} = 0.12L;\ y_c \le y \le \delta \tag{22}$$

where L is the solution of

$$u_e \frac{dL}{ds} = 1.2\,|u_\tau| \left(\frac{L}{\delta} - \frac{L^2}{\delta^2}\right) \tag{23}$$

The criterion to define the inner and outer region is given by the continuity of the eddy-viscosity or the mixing-length. From the wall outward the expression for the inner mixing length is applied until $(\ell_m)_i = (\ell_m)_o$ when $y = y_c$ or $n = n_c$.

Solution Method

Preparation of the Modeling Equations for Numerical Solution Using Keller's Box Method

After insertion of the expressions for the Reynolds stresses, the modeling equations have to be transformed into a system of first-order, nonlinear PDE's in order to use Keller's box method. This can be accomplished by using the continuity Eq. (8) to define the streamfunction ψ as

$$u = \frac{1}{r^i}\frac{\partial \psi}{\partial n} \tag{24a}$$

and

$$v = -\frac{1}{M}\frac{\partial \psi}{\partial s} \tag{24b}$$

which is related to a dimensionless streamfunction $f(\xi,\eta)$ as

$$\psi(s,n) = (\nu, u_e \xi)^{1/2} L_r^i f(\xi,\eta) \tag{25}$$

where L_r is a characteristic body length and (ξ,η) new coordinates related to (s,n) via a modified Mangler-Levy-Lees transformation, i.e.,

$$d\xi = \left(\frac{r_o}{L_r}\right)^{2i} ds \quad \text{and} \quad d\eta = \sqrt{\frac{u_e}{\nu \xi}} \left(\frac{r}{L_r}\right)^i dn \tag{26}$$

This coordinate transformation reduces the strong variations in $\delta(s)$ so that the boundary-layer edge stays about parallel to the curved wall. We now can rewrite Eqs. (8-10) as

$$f' = U = u/u_e \tag{27}$$

$$U' = V \tag{28}$$

$$[Q_1 V]' + Q_2 UV + Q_{14}(U)^2 + Q_4 fV + Q_5 fU + Q_{15} V = Q_7\left(\frac{\partial p}{\partial \xi}\right) + Q_8 U \frac{\partial u}{\partial \xi} + Q_9 V \frac{\partial f}{\partial \xi} + Q_{10} U \frac{\partial f}{\partial \xi} \tag{29}$$

where the primes denote $\partial/\partial\eta$ and the Q's are given below as

$$Q_1 = (1+\epsilon_m)\left(\frac{r}{L_r}\right)^i$$

$$Q_2 = -\frac{\partial \eta}{\partial \xi}\left(\frac{r_o}{L_r}\right)^{2i} \xi \left[(2-h)\left(\frac{L_r}{r}\right)^i - \left(\frac{L_r}{M}\right)^i\right]$$

$$Q_4 = \frac{\xi}{2}\left(\frac{r_o}{L_r}\right)^{2i}\left(\frac{L_r}{M}\right)^i\left(\frac{1}{u_e}\frac{\partial u_e}{\partial \xi} + \frac{1}{\xi}\right)$$

$$Q_5 = K\left(\frac{\nu\xi}{u_e}\right)^{1/2}\left(\frac{L_r}{r}\right)^i Q_4$$

$$Q_7 = \frac{Q_8}{\rho u_e^2};\quad Q_8 = (2-h)\left(\frac{L_r}{r}\right)^i\left(\frac{r_o}{L_r}\right)^{2i}\xi$$

$$Q_9 = -\xi\left(\frac{L_r}{M}\right)^i\left(\frac{r_o}{L_r}\right)^{2i};\quad Q_{10} = K\left(\frac{\nu\xi}{u_e}\right)^{1/2}\left(\frac{L_r}{r}\right)^i Q_9$$

$$Q_{14} = -\frac{Q_8}{u_e}\frac{\partial u_e}{\partial \xi} - Q_{10}\frac{\partial \eta}{\partial \xi} - Q_7 \rho K u_e^2 \left(\frac{\nu\xi}{u_e}\right)^{1/2}\left(\frac{L}{r}\right)^i \frac{\partial \eta}{\partial \xi}$$

$$Q_{15} = \frac{G(s,n)}{1+\epsilon_m}\left(\frac{\nu\xi}{u_e}\right)^{1/2} - Q_7 \alpha \rho \nu K \epsilon_m u_e \frac{\partial \eta}{\partial \xi}$$

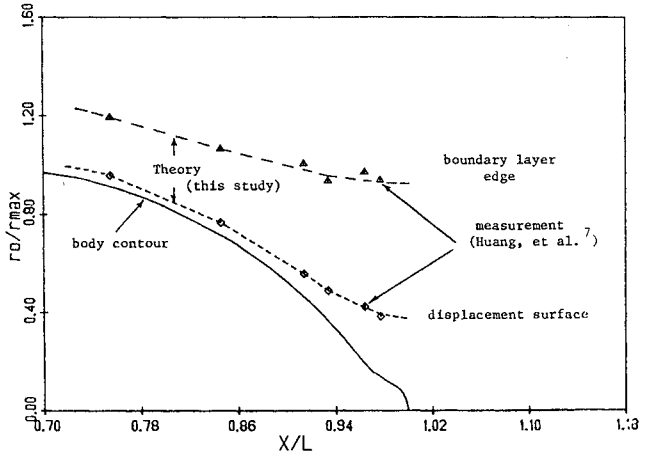

Fig. 2 Schematic of the tail of afterbody 1, computed and measured displacement thickness and boundary-layer thickness.

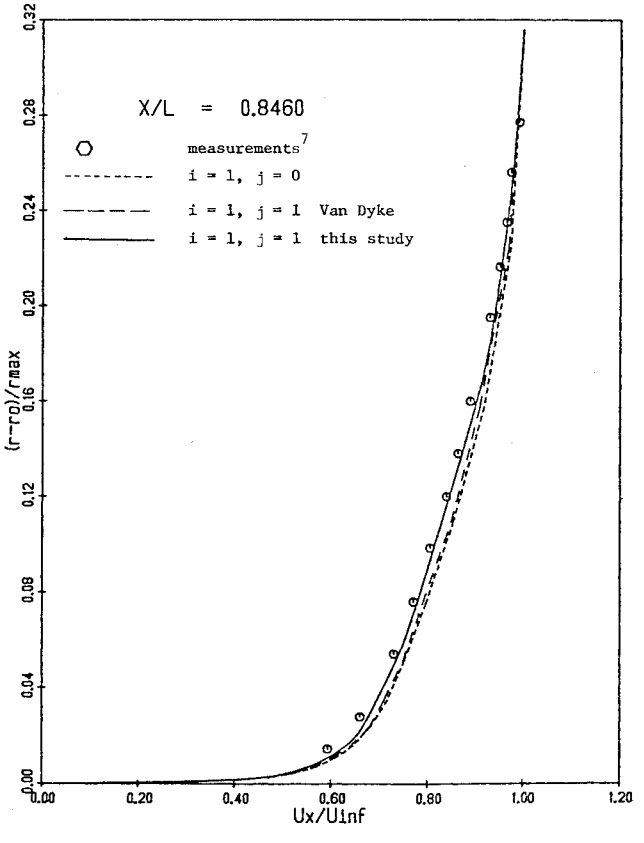

Fig. 3 Computed and measured mean axial velocity distribution across stern boundary layer at station $x/L = 0.846$.

The associated boundary conditions [Eqs. (13 and 14)] are transformed to

$$f(\xi,0)=0 \quad \text{and} \quad U(\xi,)=0 \tag{30}$$

and

$$f'=\frac{1}{1+D(\xi,\eta)} \quad \text{when} \quad \eta\to\eta_\infty \tag{31a}$$

or, in order to reduce the sensitivity of the edge boundary condition to the specification of η_∞, we differentiate Eq. (31a) to obtain

$$f''=-\frac{D_1(\xi,\eta)}{[1+D(\xi,\eta)]^2} \quad \text{when} \quad \eta\to\eta_\infty \tag{31b}$$

Combination of Eqs. (31a) and (31b) yields the edge boundary condition

$$f''+D_1 f'^2=0 \tag{32}$$

where

$$D_1(\xi,\eta)=\frac{KL_r}{r_o}\left(1+\frac{2L_r\cos\theta}{r_o^2}\sqrt{\frac{\nu\xi}{u_e}}\eta\right)^{-1/2}\sqrt{\frac{\nu\xi}{u_e}} \tag{33}$$

and

$$D(\xi,\eta)=-\frac{Kr_o}{\cos\theta}\left[1-\left(1+\frac{2L_r\cos\theta}{r_o^2}\sqrt{\frac{\nu\xi}{u_e}}\eta\right)^{1/2}\right] \tag{34}$$

For a flat plate, $D=D_1=0$ so that $f'=1$.

There is a large number of numerical schemes available for solving (parabolic) boundary-layer flow problems. Eghlima[28] discussed the merits of Keller's box method with an improved (i.e., more flexible and computationally more efficient) equation solver over other competitive algorithms such as the Crank-Nicolson finite difference method or the Galerkin finite element method.

Equations (27-29) are discretized for an arbitrary rectangular grid using centered difference quotients and averages at the midpoints of the net rectangles. The mesh of varying density for the stern of the test bodies (afterbodies 1 and 5) discussed in the next section, are 50 and 66 grid points in the streamwise and 49 and 56 in the normal direction. Three iterations were required to obtain the displacement surface. The main sources of computational errors are caused by round-off error, iteration error, the error induced due to linearization, and the truncation error of the numerical scheme. The first three errors are smaller than the fourth one because the program is in double precision and the iteration and linearization errors are of the order of 10^{-4}. The local accuracy of the numerical algorithm is $\mathcal{O}(h^2)$ where h is equal to the grid spacing, due to the centered-difference quotients employed. To check the overall accuracy of the numerical solution, we have divided the mesh spacing by two and four and the results indicated that the global error is $\mathcal{O}(h^2)$ as well. The distribution of the pressure coefficient on the tail of the test bodies was computed with the displacement body method discussed by Wang and Huang.[18] They have shown that the maximum error in the static pressure associated with this method is less than 2% of the dynamic pressure. Once the pressure distribution is known along the displacement surface, the normal pressure variation at each station x/L is obtained from our n-momentum equation.

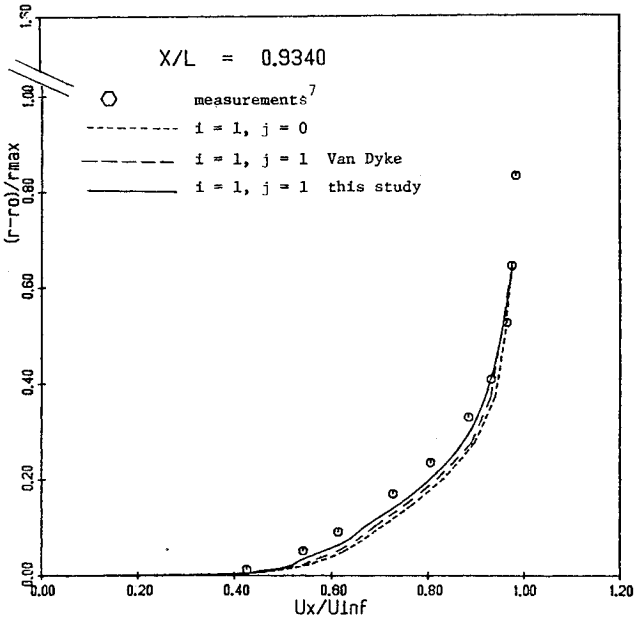

Fig. 4 Computed and measured mean axial velocity distribution across stern boundary layer at station $x/L=0.934$.

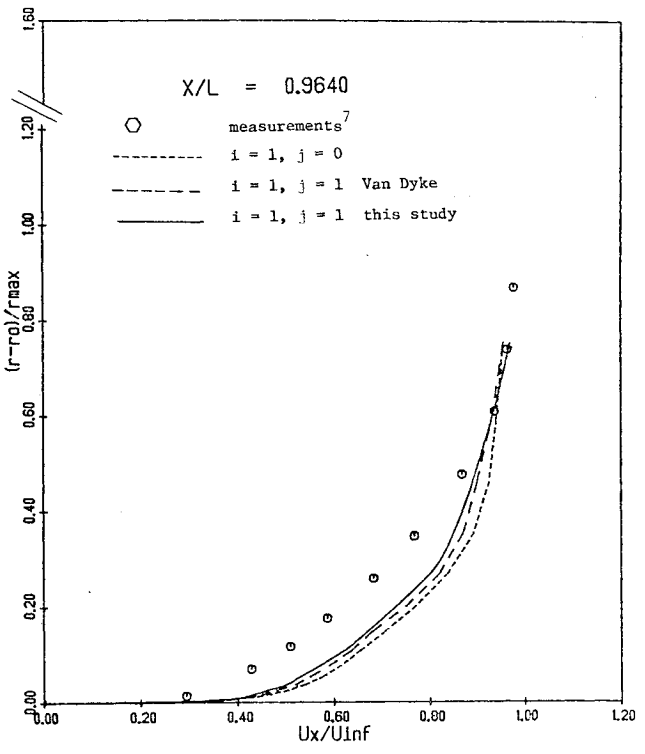

Fig. 5 Computed and measured mean axial velocity distribution across stern boundary layer at station $x/L=0.964$.

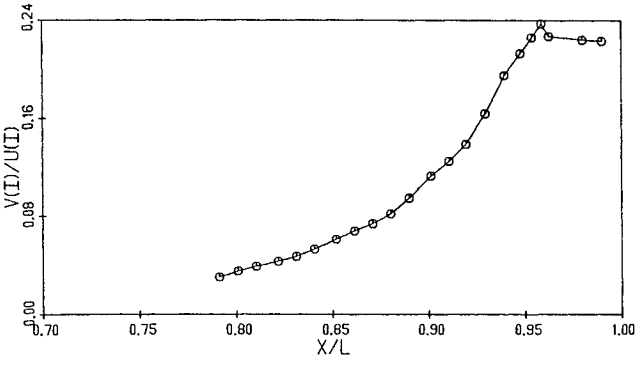

Fig. 6 Computed maximum normal velocity vs tangential velocity along the body.

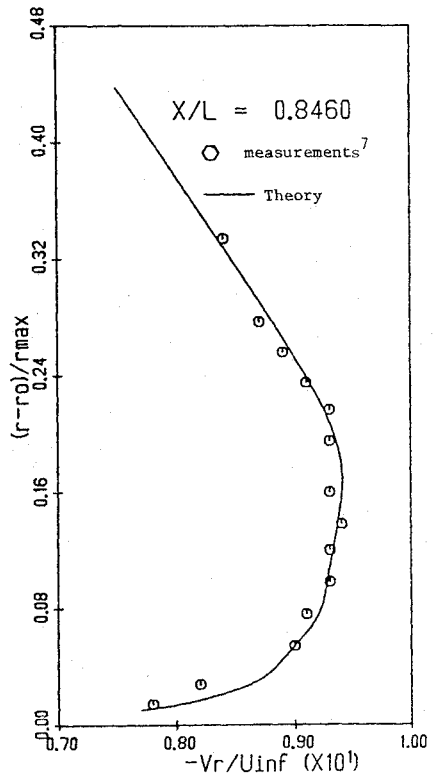

Fig. 7 Computed and measured mean radial velocity distribution across stern boundary layer at station $x/L = 0.846$.

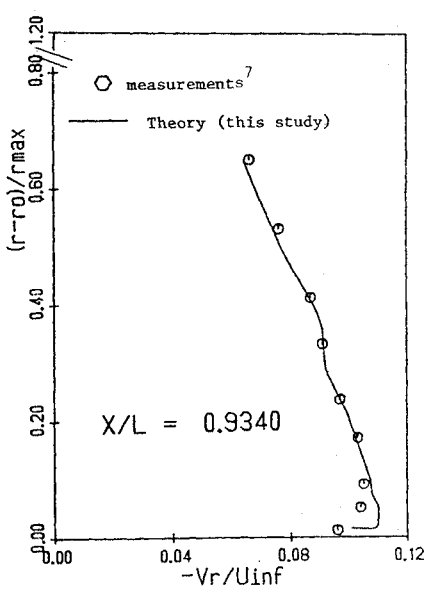

Fig. 8 Computed and measured mean radial velocity distribution across stern boundary layer at station $x/L = 0.934$.

Results and Conclusions

Simulation Results and Comparison with Measured Data Sets

Huang et al.[7] have conducted their measurements with several axisymmetric, antiseparation bodies exhibiting longitudinal and transverse curvatures. To the authors' best knowledge, their experiments generated the most complete and reliable sets of data for this special class of complex flows. Reynolds numbers ($Re = U_\infty L_r/\nu$) in these case studies were 6.8×10^6 for afterbody 1 corresponding to $U_\infty = 30.48$ m/s and $L_r = 3.066$ m and 9.3×10^6 for afterbody 5 with $U_\infty = 40.64$ m/s and $L_r = 2.87$ m. The diameter of the parallel middle section is 27.94 cm for both test bodies.

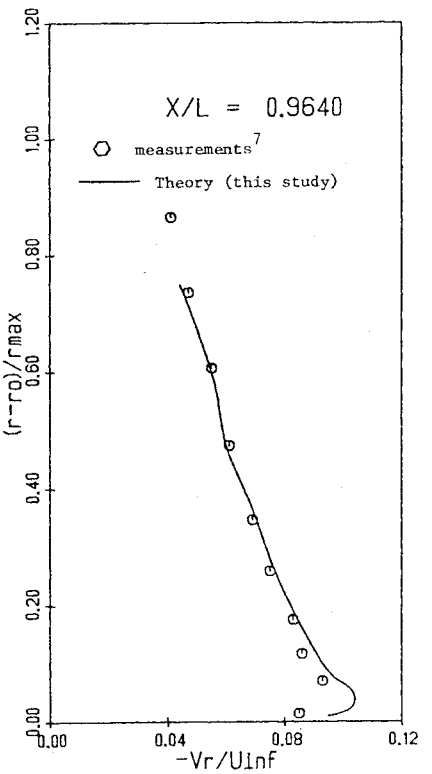

Fig. 9 Computed and measured mean radial velocity distribution across stern boundary layer at station $x/L = 0.964$.

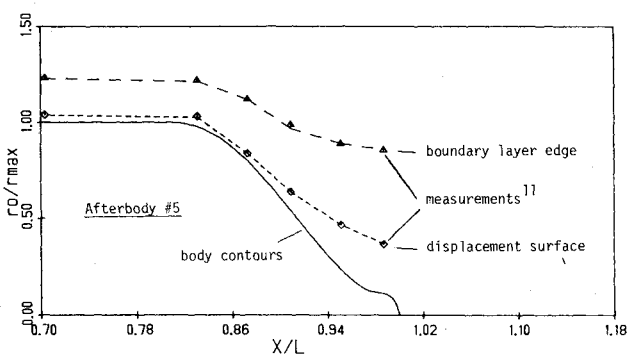

Fig. 10 Schematic of the stern of afterbody 5, computed and measured displacement surface, and boundary-layer thickness.

To evaluate and compare the new set of boundary-layer equations with measurements and other theoretical modeling efforts, we have divided the results into two parts according to comparisons with afterbodies 1 and 5.

Afterbody 1: Comparison of Results from Different Modeling Equations with Measured Data Sets

Figure 2 shows a comparision between computed (this study) and measured[7] displacement thickness and boundary-layer thickness, in which the agreement between theory and measurements is excellent for both parameters. Figures 3-5 compare the measured mean axial velocity distribution across the stern boundary layer with computed results from the turbulent version of Van Dyke's higher-order boundary layer equations,[6] our new improved equations, and boundary-layer equations with only transverse curvature effect. To compute these results we have used an eddy-viscosity model in which transverse curvature has been taken into account only, with no correction due to the thickening of the boundary layer. Therefore, the differences between the results are only due to the existence of longitudinal curvature terms in the momentum equation. Figures 3-5 and 7-9 demonstrate that our new second-order boundary-layer equations perform well

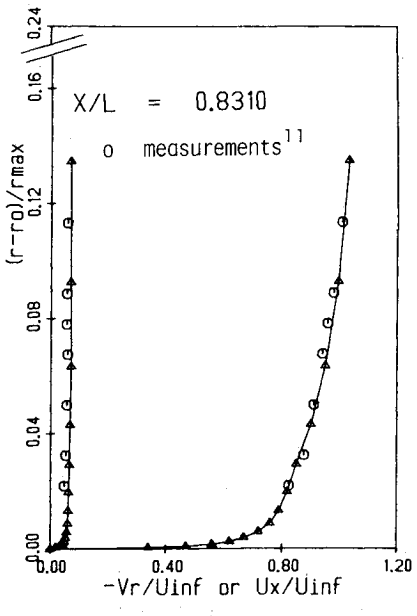

Fig. 11 Axial and radial velocity profiles for afterbody 5 at station $x/L = 0.831$.

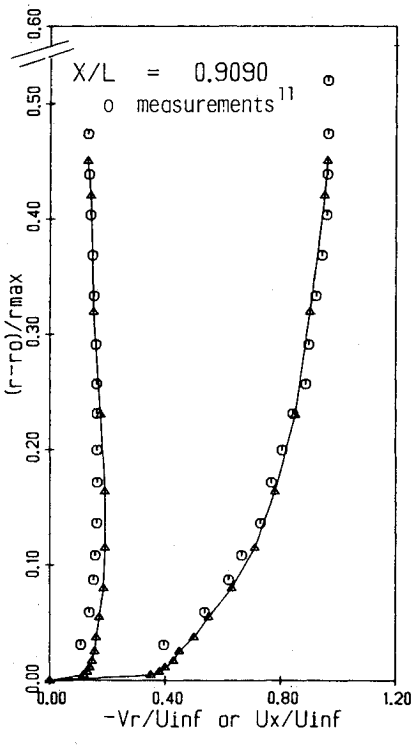

Fig. 12 Axial and radial velocity profiles for afterbody 5 at station $x/L = 0.909$.

in computing velocity profiles when $\delta/R \approx \mathcal{O}(0.1)$, provided that $v \ll u$. It is interesting to note that Huang et al.[7] used thin shear layer equations[19] with transverse curvature effect only to compute the velocity profiles for the same flow system. In addition, they included a correction factor in the eddy viscosity model which was based on experimental observations of the same flow system. In contrast, our new equations with transverse and longitudinal curvature effects produce without any algebraic correction for the turbulence model slightly better results than Huang et al.[7] as demonstrated in Ref. 22.

Figure 5 shows that at $x/L = 0.964$ the agreement between measurements and computation is not good enough. The

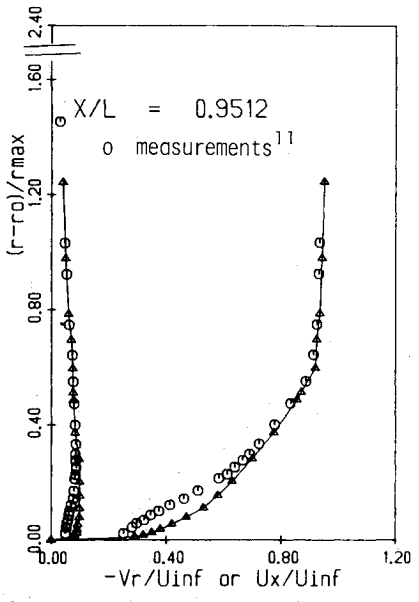

Fig. 13 Axial and radial velocity profiles for afterbody 5 at station $x/L = 0.9512$.

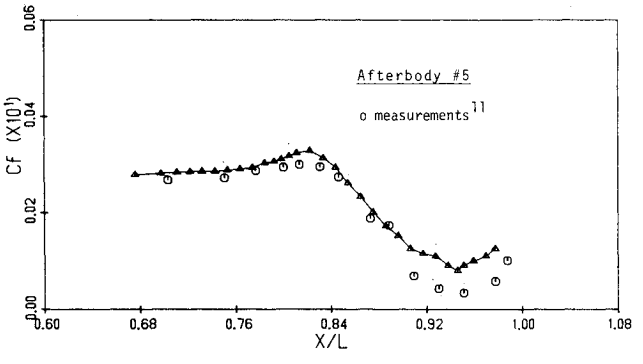

Fig. 14 Distribution of skin friction coefficient for afterbody 5.

main reason for these discrepancies downstream of $x/L > 0.94$ is that the basic assumption $v/u \ll 1$ is not valid anymore at the very end of the submerged body (Fig. 6). Indeed, whenever the streamlines are approximately parallel to the body surface, i.e., $v \ll u$ which is incorporated in Eq. (4), the new second-order boundary-layer equations give excellent results as also shown in the next case study with afterbody 5. Thick turbulent boundary-layer flows with regions where $v = \mathcal{O}(u)$ will be discussed in a forthcoming paper.[29]

Figures 7-9 show the comparison between predicted normal velocity profiles and measured data points at the three stations $x/L = 0.846$, 0.934, and 0.964. The matching is very good mainly due to the incorporation of the n-momentum equation which is usually neglected for this class of flows.

Afterbody 5: Comparison of Experimental and Computational Results Employing MLH Submodels with Curvature Effects

Afterbody 5 has a more gentle curvature transition from convex to concave than afterbody 1. Figure 10 depicts the body contour, the displacement surface, and the (thick) turbulent boundary layer. The zero-equation closure model used reflects longitudinal as well as transverse curvature effects as given in Eqs. (19-23).

In Figs. 11-13, the axial and radial velocity profiles are plotted on the same scale for various downstream stations x/L. In the end zone $x/L > 0.91$ slight discrepancies between measured and predicted profiles near the wall can be detected which resurface in the distribution of the skin friction coefficient shown in Fig. 14. The last graph should be viewed together with the particular body contour given in Fig. 10.

Conclusions and Future Work

The present simulation results are obtained with an extended mixing length model reflecting transverse and longitudinal curvature effects and a new set of higher-order boundary layer equations. This relatively simple modeling approach is very accurate in predicting the behavior of attached thick turbulent boundary layers past axisymmetric bodies as long as the streamlines are approximately parallel to the wall. Incorporation of the n-momentum equation in the calculation procedure, reflecting the influence of normal velocity and static pressure variations, has resulted in good predictions of the normal component of the mean flow velocity. However, local discrepancies for both velocity profiles when compared with laboratory observations still exist at the very end of the submerged bodies, i.e., in the region $0.94 < x/L < 1.00$. As discussed earlier, the reason for the differences include the assumption that $v \ll u$ which leads to a rather simplified n-momentum equation which cannot fully represent the flow dynamics at the very end of the submerged body or very close to the point of separation.

From the observed rapid variations in the mixing-length distributions, it would appear to be desirable to replace the MLH by a two-equation model. However, such existing turbulence models have to be modified to account for the extra rates of strain stemming from such effects as body curvature and streamline convergence which are present in the case examined here. In addition to the problem of incorporating a more general turbulence model, an accurate treatment of thick boundary-layer developments up to and after the line of separation has to take into account the effects of normal pressure gradients as well as the fact that $v = \mathcal{O}(u)$. Results of such case studies and comparison with measured data sets will be reported in forthcoming papers.

Acknowledgment

This research was supported in part by the Office of Naval Research, ONR Grant N 00014-82-K-0465 (NR 062-738).

References

[1] Van Dyke, M., "Higher Approximation in Boundary-Layer Theory. Part 1. General Analysis," *Journal of Fluid Mechanics,* 1962, p. 161.

[2] Van Dyke, M., "Higher-Order Boundary-Layer Theory," *Annual Review of Fluid Mechanics,* 1969, p. 265.

[3] Meroney, R. N. and Bradshaw, P., "Turbulent Boundary-Layer Growth Over a Longitudinally Curved Surface," *AIAA Journal,* Vol. 13, 1975, p. 11.

[4] Rastogi, A. K. and Whitelaw, J. H., "Procedure for Predicting the Influence of Longitudinal Curvature on Boundary-Layers," ASME Paper 71-WA/FE-37, New York, 1971.

[5] Patel, V. C., "A Simple Integral Method for the Calculation of Thick Axisymmetric Turbulent Boundary Layers," *Aeronautical Quarterly,* Vol. 25, 1974.

[6] Cebeci, T., Hirsh, R. S., and Whitelaw, J. H., "On the Calculation of Laminar and Turbulent Boundary-Layers on Longitudinally Curved Surfaces," *AIAA Journal,* Vol. 17, 1979, p. 4.

[7] Huang, T. T., Santelli, N. and Belt, G., "Stern Boundary-Layer Flow on Axisymmetric Bodies," 21st Symposium on Naval Hydrodynamics, Washington, D.C., June 5-9, 1978, p. 127, available from National Academy of Sciences, Washington, D.C., 1979.

[8] Patel, V. C. and Choi, C. H, *Turbulent Shear Flows II,* edited by L. J. S. Bradbury, et al., Springer-Verlag, New York, 1980.

[9] Gibson, M. M., Jones, W. P., and Younis, B. A., "Calculation of Turbulent Boundary-Layers on Curved Surfaces," *Physics of Fluid,* Vol. 24, 1981, p. 3.

[10] Kleinstreuer, C. and Eghlima, A., "New Second-Order Boundary-Layer Equations for Flow Past Surfaces with Strong Curvature Effects," *Mathematics and Computers in Simulation,* Vol. 27, No. 1, 1985.

[11] Huang, T. T., Groves, N. C., and Belt, G., "Boundary-Layer Flow on an Axisymmetric Body with an Inflected Stern," DTNSRDC-80/064, 1980.

[12] Gillis, J. C. and Johnston, J. P., *Turbulent Shear Flows II,* edited by L. J. S. Bradbury et al., Springer-Verlag, New York, 1980.

[13] Smith, A. J., Young, S. T., and Bradshaw, P., "The Effect of Short Regions of High Surface Curvature on Turbulent Boundary-Layer," *Journal of Fluid Mechanics,* Vol. 94, 1979, p. 209.

[14] Patel, V. C. and Lee, Y. T., "Thick Axisymmetric Boundary Layers and Wakes: Experiment and Theory," Paper 4, *International Symposium on Ship Viscous Resistance,* Göteborg, Sweden, 1978.

[15] Shivaprasd, B. G. and Ramaprian, B. R., "Turbulence Measurements in Boundary-Layers Along Mildly Curved Surfaces," *Journal of Fluid Engineering, Transactions of the ASME,* Vol. 100, 1978.

[16] So, R. M. C. and Mellor, G., *Journal of Fluid Mechanics,* Vol. 60, 1973, p. 43.

[17] Patel, V. C., "Measurement in the Thick Axisymmetric Turbulent Boundary-Layer Near the Tail of a Body of Revolution," *Journal of Fluid Mechanics,* Vol. 63, 1974.

[18] Wang, H. T. and Huang, T. T., "Calculation of Potential Flow/Boundary-Layer Interaction on Axisymmetric Bodies," Ship Performance Dept., David W. Taylor Naval Ship R&D Center, Bethesda, Md., 1979.

[19] Cebeci, T. and Smith, A. M. O., *Analysis of Turbulent Boundary Layers,* Academic Press, New York, 1974.

[20] Bradshaw, P., personal communication, Imperial College, London, U.K., 1982.

[21] Patel, V. C., "On the Equations of a Thick Axisymmetric Turbulent Boundary Layer," The Univ. of Iowa, IIHR Rept. 143, Jan. 1973.

[22] Kleinstreuer, C., Flaherty, J. E., and Eghlima, A., "Computer Simulation of Thick Incompressible Boundary Layers," *Proceedings of International Conference on Numerical Methods in Laminar and Turbulent Flow,* edited by C. Taylor, J. A. Johnson, and W. R. Smith, Pineridge Press, Swansea, U.K., 1983.

[23] von Kármán, T. H., "Mechanische Ähnlichkeit und Turbulenz," *Proceedings of Third International Congress Applied Mechanics,* Stockholm, Pt. 1, 1931, p. 85.

[24] Boussinesq, J., "Théorie de l'écoulement tourbillant," *Mem. Pre. Par. Div. Sav.,* Vol. 23, Paris, 1877.

[25] Eide, S. A. and Johnston, J. P., Thermoscience Div., Mechanical Eng. Dept., Stanford University, Calif., Rept. PD-19, 1974.

[26] Van Driest, E. R. *Aeronautical Engineering Review,* Vol. 15, 1956, p. 26.

[27] Pletcher, R. H., "Prediction of Incompressible Turbulent Separating Flow," *Journal of Fluid Engineering,* Vol. 100, 1978, p. 427.

[28] Eghlima, A. "Theoretical Analysis and Computer Simulation of Thick Incompressible Laminar/Turbulent Boundary Layer Flows Along Curved Surfaces," Ph.D. Thesis, Rensselaer Polytechnic Institute, Troy, N.Y., 1982.

[29] Kleinstreuer, C. and Eghlima, A. "Numerical Analysis of Attached Laminar and Turbulent Shear Layers with Streamline Curvature Effects," *Numerical Techniques for Fluid Flow,* edited by C. Taylor et al., Vol. V, Pineridge Press, Swansea, U.K., 1984.